VIROLOGY 225, 65–71 (1996)
ARTICLE NO. 0575

Which Controls Antigenicity and Host Range

ANTONIO L. LLAMAS-SAIZ,*,[1] MAVIS AGBANDJE-MCKENNA,*,[2] JOHN S. L. PARKER,† A. T. M. WAHID,† COLIN R. PARRISH,† and MICHAEL G. ROSSMANN*,[3]

*Department of Biological Sciences, Purdue University, West Lafayette, Indiana 47907-1392; and †James A. Baker Institute, New York State College of Veterinary Medicine, Cornell University, Ithaca, New York 14853

Received June 3, 1996; accepted August 5, 1996

A single mutation in canine parvovirus (CPV) of VP2 residue 300 from alanine to aspartic acid causes a loss of canine host range and alters the antigenic properties of the virus. The three-dimensional structure of this mutant has been solved to 3.25 Å resolution. Crystals of full particles were triclinic, with cell dimensions of $a = 267.6$, $b = 268.5$, $c = 274.3$ Å, $\alpha = 61.9$, $\beta = 62.6$, and $\gamma = 60.2°$. The native structure of CPV was used as an initial model. Phases were improved by real-space electron density averaging. In spite of the relative low percentage of observed reflections (32.5% of the data between 15.0 and 3.25 Å resolution), the presence of 60-fold noncrystallographic redundancy allowed the averaging procedure to converge smoothly. The mutant aspartic acid at residue 300 forms a salt bridge with Arg81 in an icosahedrally threefold-related subunit, inducing local changes within the antigenic site B on the CPV surface. In addition, the loop between residues 359 and 374 adopts a conformation similar to that displayed by feline panleukopenia virus. The ability of the Ala300 → Asp mutant to evade antibody binding can be associated with the change of charge distribution and structure in the antigenic binding site. The variation in host range behavior may be due to the increased stability as a result of formation of the salt bridge between adjacent subunits.

INTRODUCTION

Canine parvovirus (CPV) is a member of the family *Parvoviridae.* CPV was first recognized in 1978 as the cause of a new disease of dogs and appears to be a host range variant of feline panleukopenia virus (FPV) or a closely related virus of another carnivore (Parrish, 1990; Truyen *et al.,* 1995). Naturally variant strains of CPV differ in their ability to infect cat cells, although only a small number of amino acids are changed in their capsid protein sequence (Parrish *et al.,* 1991; Truyen *et al.,* 1996). Parvovirus replication occurs only in actively proliferating cells (Siegl, 1984), leading to disease, primarily through effects on tissues containing mitotically active cells.

The nonenveloped parvovirus capsid has $T = 1$ icosahedral symmetry, with a diameter of approximately 260 Å, that encapsidates the ssDNA genome composed of about 5200 bases. The DNA-containing virions have a molecular weight between 5.0×10^6 and 6.2×10^6 Da, while empty capsids have a molecular weight of 4.2×10^6 Da. In CPV, the genome encodes two structural proteins, VP1 and VP2, formed by alternative splicing of the same messenger RNA (Jongeneel *et al.,* 1986). VP1 contains 143 additional residues compared to VP2. A third protein, VP3, occurs only in full, DNA-containing, particles and is generated by the proteolytic cleavage of approximately 17 residues from the N-terminus of VP2 (Cotmore and Tattersall, 1987). About 90% of the capsid is formed by a combination of VP2 and VP3 subunits, while the remaining subunits are VP1. The three-dimensional structures of CPV (Tsao *et al.,* 1991) and FPV (Agbandje *et al.,* 1993) have been solved using X-ray crystallography at 3.3 Å resolution or better. The first 36 amino acids of VP2 are not visible in their respective electron density maps. About one-third of the residues in the protein of these viruses constitute an eight-stranded, antiparallel, β-barrel motif usually found in viral capsid proteins (Rossmann and Johnson, 1989). The other two-thirds form insertions (loops 1 to 4) between the β-strands of the β-barrel, some of which give rise to the characteristic topology of the viral surface. Features of the capsid structure include a cylindrical channel along each of the fivefold axes surrounded by canyon-like depressions, small spikes around the threefold axes, and "dimple-like" depressions at the twofold axes.

Two dominant neutralizing antigenic sites, termed sites A and B, have been mapped on the CPV surface using both escape mutant analysis and peptide epitope mapping (Rimmelzwaan *et al.,* 1990; López de Turiso *et al.,* 1991; Langeveld *et al.,* 1993; Strassheim *et al.,* 1994). Site A is

[1] Present address: Departamento de Cristalografia, Instituto de Quimica-Fisica "Rocasolano", CSIC, Serrano 119, 28006 Madrid, Spain.
[2] Present address: Department of Biological Sciences, University of Warwick, Coventry CV4 7AL, United Kingdom.
[3] To whom correspondence and reprint requests should be addressed.

0042-6822/96 $18.00

TABLE 1

Interaction between the HyHel 5 Fab Model and the CPV Surface

CDR[a]	HyHel 5[b]	A3B10[c]	CPV[d]
L1	N30	S35	T391
L2	—		
L3	R92	Y97	T390, T391
H1	T28, S30, D31, Y32, W33	S28, T30, D31, Y32, I33	N85, M87, N231, I232, Y233, G299, A300, T301, F303
H2	L52	N52	Q296, S297, T301, N302
H3	N100, Y101	G100, Y101	
CPV escape mutations:			G299E, A300V, A300D, N302D
Mutations that do not affect the ability of A3B10 to neutralize CPV:			A300G

[a] CDR, complimentarity determining region.
[b] At least one nonhydrogen atom within these residues is within 5.0 Å of an atom on the CPV surface.
[c] Equivalent residues in A3B10.
[d] Bold-faced residues can carry escape mutations.

on the threefold spike, involving loops 1, 2, and 4. Site B is on a "shoulder" of the threefold spike near a ridge between the canyon and the dimple on the twofold axis. Additional antigenic sites have also been identified by peptide epitope mapping, including the externalized amino end of VP2 (López de Turiso *et al.,* 1991; Langeveld *et al.,* 1993).

A cryoelectron microscopy structure has been reported (Wikoff *et al.,* 1994) of wild-type CPV strain d (CPV-d), complexed with the Fab of neutralizing monoclonal antibody (MAb) A3B10 (antibody 8 in Strassheim *et al.,* 1994). This antibody recognized antigenic site B. The electron density obtained of the complex was fitted with the known structures of CPV and the homologous HyHel 5 Fab structure. This permitted the mapping of the footprint of the bound antibody on the viral surface and an analysis of the interaction of specific residues in the interface (Table 1) based on the aligned sequences of A3B10 and HyHel 5 (Wikoff *et al.,* 1994). A number of escape mutations (Table 1) had been isolated and used for mapping the neutralizing epitopes of CPV.

A mutant of CPV (CPV 102/10), derived by extended passaging in canine and feline cell lines, was found to be altered in host range and antigenic type (Parrish and Carmichael, 1986). Recombination analysis mapped the host range and antigenic mutations to a region within the VP2 gene. That region encoded four amino acid changes (Lys271 → Arg, Ala300 → Asp, Thr301 → Ile, Val316 → Ile). These mutations were prepared as single changes by site-directed mutagenesis. The mutant Ala300 → Asp (designated mutant vBI394) was not recognized by several MAbs that bind to antigenic site B in the parental virus. Furthermore, this mutant also lost its ability to replicate in certain canine cells. The structural analysis of this mutant is reported here.

METHODS AND RESULTS

Preparation and analysis of mutant virus

A site-directed mutation of nucleotide 3685 from C to A (codon GCT to GAT) was prepared using the oligonucleotide 5′-GAAGGAGATACTAACT-3′ by the method of Kunkel (1985) . The region containing the mutation between *Spe*I and *Eco*RV sites was sequenced and used to replace the corresponding region of the infectious plasmid clone of CPV-d (Parrish, 1991). The plasmid was transfected into NLFK cells by electroporation (Chang *et al.,* 1992). The resultant virus (Ala300 → Asp, vBI394) was found to be nonreactive with most MAbs which recognize the antigenic site B (Strassheim *et al.,* 1994).

The type-I MDCK cell clone AA7 (Nichols *et al.,* 1988) obtained from Dr. W. W. Young (University of Kentucky) was found to be susceptible to infection by wild-type CPV isolates. The NFLK, A72, or MDCK-AA7 cells were inoculated with approximately 0.2 m.o.i. of mutant vBI394 or wild-type CPV-d. After 72 hr, the cells were lysed into 0.15 *M* NaCl, 10 m*M* Tris–HCl (pH 7.5), 10 m*M* EDTA, 2% (w/v) sodium dodecyl sulfate, with 250 μg/ml of proteinase K, incubated for 40 min at 60°, extracted twice with phenol and ethanol precipitated. The total recovered DNA was electrophoresed in 1% agarose gels containing 0.5 μg/ml ethidium bromide and then transferred to nitrocellulose membranes by Southern blotting. The viral DNA was then detected by hybridization with a full-length genomic probe labeled with [^{32}P]dCTP. Although CPV-d replicated well in feline (NLFK) or canine (A72 or MDCK-AA7) cells, the mutant virus replicated well only in NLFK cells, to a limited extent in A72 cells, and not at all in the MDCK-AA7 cells (Fig. 1).

X-ray structure determination

CPV vBI394 mutant (Ala300 → Asp) was propagated and purified using methods described by Agbandje *et al.* (1993). Crystals were grown using the hanging drop vapor diffusion method (McPherson, 1982) with the same conditions as had been used to crystallize wild-type CPV (Tsao *et al.,* 1992). X-ray diffraction data were collected at the F1 station of the Cornell High Energy Synchrotron Source (CHESS) employing an oscillation camera and

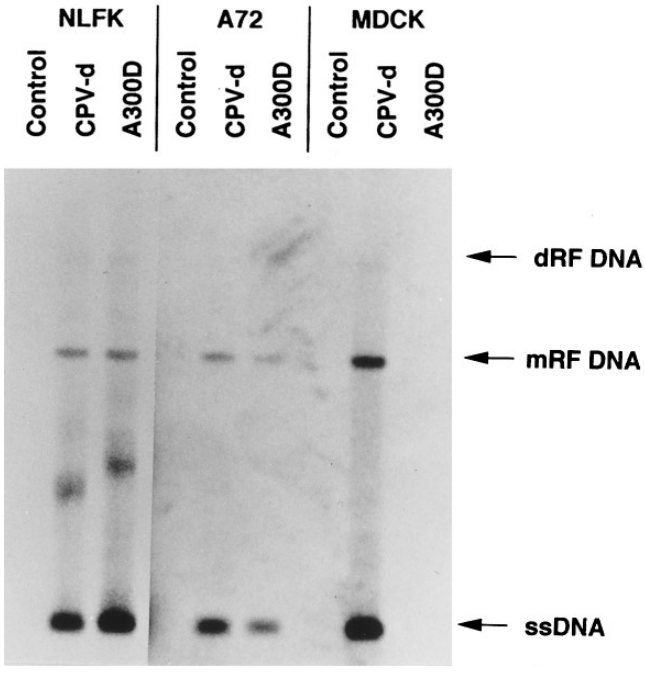

FIG. 1. Viral DNA replication in NLFK, A72, and MDCK cell lines. Cellular DNA isolated from the cells 72 hr after inoculation with wild-type CPV-d, vBI394 (mutant Ala300 → Asp mutant), or control mock-inoculation was electrophoresed in a 1% agarose gel, transferred to a nylon membrane, and probed with a ^{32}P-labeled viral DNA fragment. Viral single-stranded DNA (ssDNA), as well as monomeric (mRF) and dimeric (dRF) replicative forms of RF DNA, are indicated.

Fuji imaging plates. The crystal-to-imaging plate distance was 300 mm and the oscillation angle was 0.4° with a wavelength of approximately 0.908 Å. The temperature of the crystal was kept constant at 4° to minimize radiation damage. All 100 oscillation images were collected from a single crystal (about 1 mm in diameter) that was exposed at three different positions along its length. The diffraction pattern extended to the edges of the imaging plates, corresponding approximately to a maximum resolution of 2.7 Å.

The crystal orientation matrix for the first image was obtained using the program DENZO (Otwinowski, 1993). This matrix was then used to process and scale all the images with the Purdue data processing package (Rossmann, 1979; Rossmann *et al.,* 1979). The orientation and mosaicity for each image and overall cell dimensions were further postrefined, giving rise to cell parameters $a = 267.6, b = 268.5, c = 274.3$ Å, $\alpha = 61.9$, $\beta = 62.6$, and $\gamma = 60.2°$ in space group $P1$. The vertical and horizontal effective mosaic spread changed from around 0.07° and 0.03° to about 0.25° and 0.13°, respectively, during the data collection. The final data set contained 32.5% of the total available data to 3.25 Å resolution with an R_{merge} of 9.0% after rejecting reflections with $I < 2\sigma(I)$.

Assuming one viral particle in the triclinic $P1$ cell, the Matthews coefficient, V_M, (Matthews, 1968) is 2.4 Å^3/Da. The origin of the unit cell was chosen to be at the particle center. The orientation of the virus was determined by self-rotation function searches for noncrystallographic twofold, threefold, and fivefold rotation axes. The [P] matrix was determined by making a least-squares fit to icosahedral symmetry axes in a standard orientation (Agbandje *et al.,* 1993) to the high resolution self-rotation function peaks and was found to be

$$[P] = \begin{pmatrix} 0.8727 & 0.0652 & 0.4838 \\ -0.3961 & 0.6738 & 0.6237 \\ -0.2853 & -0.7360 & 0.6139 \end{pmatrix}$$

The r.m.s. deviation of the rotation axes at a radius of 140 Å was 0.19 Å. The [P] matrix relates the symmetry elements of an icosahedron placed in a standard orientation (the *h*-cell) with its actual disposition in the real structure (the *p*-cell) by X = [P]Y, where X and Y are Cartesian coordinates in the standard and real cells, respectively (Rossmann *et al.,* 1992). Y is an orthogonal system in the triclinic cell, as defined by Rossmann and Blow (1962).

The final averaged electron density map of the previously determined native CPV-Alabama structure (Tsao *et al.,* 1991) was placed in the standard orientation into an *h*-cell. The electron density for this CPV-Alabama particle was then reoriented and placed into the triclinic cell, using the previously determined [P] matrix. The resulting electron density map was Fourier back-transformed and the initial R-factor and correlation coefficient (CC) were found to be 45.4% and 0.42, respectively. Subsequently, 20 cycles of electron density averaging and solvent flattening were performed using a weighting scheme (Arnold and Rossmann, 1988) and using F_{calc} values where there were no observed reflections. A spherical mask was used which had inner and outer radii of 70 and 140 Å, respectively. The electron density was set to its mean value in the solvent and nucleic acid regions. The R-factor and overall CC improved to 15.9% and 0.91, respectively.

Although the percentage of observed data is rather small, the final electron density map obtained for the mutant virus shows that the bias of the initial model had been removed. The refined atomic model of CPV-Alabama (Chapman and Rossmann, 1996) was used as a guide to model the electron density map of the mutant virus. Figure 2 shows the electron density corresponding to the side chain of Asp300, together with the surrounding conformational changes. The biggest differences between the mutant virus and CPV-Alabama, as much as 7.5 Å in C_α positions, occur between Gly299 and Thr301, between Gly360 and Asp373, between Thr390 and Glu393, and at Met518 (Table 2). The changes in the polypeptide between residues 390 to 393 of a twofold-related subunit are correlated with the conformationally altered residues around the mutated Asp300 (Fig. 3). Surprisingly, residues 360 to 373 display

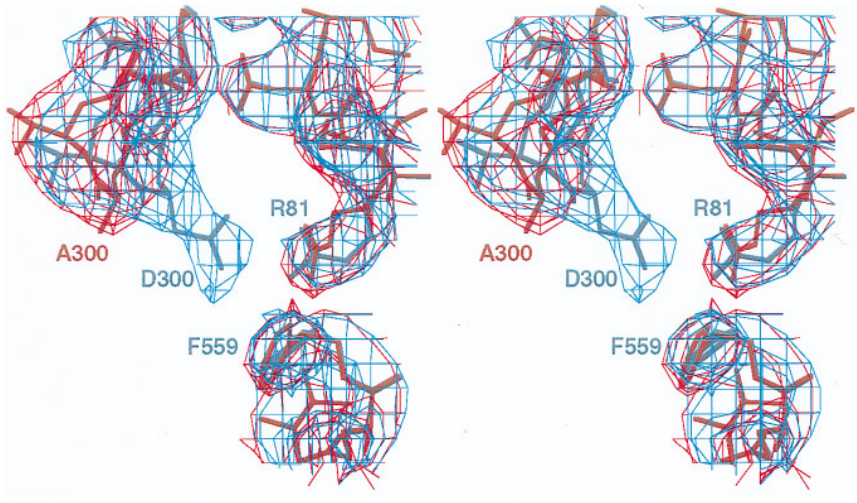

FIG. 2. Superposition of the electron densities and atomic models of CPV-Alabama (red) and the Ala300 → Asp mutant of CPV-d (blue) showing the modification in the conformation of the loop induced by the salt bridge between Asp300 and Arg81 of a threefold-related subunit.

a conformation similar to that found for FPV (Agbandje *et al.,* 1993), instead of the partially disordered structure found in CPV-Alabama (Table 2).

The atomic coordinates for the mutant virus will be deposited with the Brookhaven Protein Data Bank.

DISCUSSION

The mutation of Ala300 → Asp was introduced into CPV-d genome, which altered the structure of the antigenic site B and also reduced or eliminated the ability of the virus to replicate in canine MDCK-AA7 cells. The mutation at residue 300 is at a different region of the capsid structure from other changes between CPV and FPV (Asn93 → Lys and Asn323 → Asp) that determine the ability of CPV to replicate in cat cells (Chang *et al.,* 1992; Agbandje *et al.,* 1993). Residue 300 is variable among virus isolates, being an alanine in most FPV and CPV type-2 strains, but it is a glycine in the most recent strains of CPV (CPV type-2a and CPV type-2b) and a valine in mink enteritis type-2 virus isolates (Truyen *et al.,* 1995).

TABLE 2

Changes in Structure between CPV-Alabama, CPV-d Mutant, and FPV for All Residues Where the C_α Displacement between the Mutant and CPV-Alabama Is Greater Than 1.0 Å

Residue	Mut:CPV-Alabama	Mut:FPV	CPV-Alabama:FPV
299	1.1	1.4	0.4
300	2.2	1.8	0.4
301	1.4	1.0	0.6
360	4.0	0.4	3.8
361	2.5	0.5	2.5
362	4.7	1.0	4.9
363	3.4	0.6	3.8
364	1.8	2.0	0.9
365	4.6	2.6	5.0
366	1.5	1.9	0.8
367	7.5	1.1	6.6
368	7.0	0.5	6.9
369	7.0	0.8	7.3
370	4.9	0.3	4.6
371	5.7	0.5	5.7
372	5.1	0.2	4.9
373	4.5	0.5	4.7
390	1.0	0.1	1.1
391	1.7	0.8	1.1
392	1.6	0.8	1.2
393	1.4	0.9	0.7
518	1.3	1.9	0.9

Earlier studies of the CPV structure were of a strain obtained from the University of Alabama at Birmingham (CPV-Alabama). This virus differs from CPV-d by having a lysine, instead of a glutamine, at residue 386 in VP2 (Table 3). Comparison of the structures of CPV-Alabama with the mutant Ala300 → Asp showed conformational changes larger than 1 Å in their C_α positions in four separate regions (Table 2). Two of these regions (299–301 and 390–393) are around the positions of the two altered amino acids at position 300 and 386, respectively. Most of the structurally changed residues occur on the viral surface and include much of the epitope B (Fig. 4). The two altered residues (300 and 386) are about 19 Å apart and are both associated with this epitope. Thus, it was not immediately clear which altered residue caused which of the conformational changes.

The amino acid sequence of FPV differs from CPV-Alabama by 10 residues in VP2, but is the same as CPV-d at position 386 (Table 3). The CPV-d mutant has a Gln at position 386, the same as occurs in FPV, but not in CPV-Alabama. The structure of the mutant in the vicinity of residue 386 (residues 390–393) is similar to FPV, but not to CPV-Alabama (Table 2). Thus, the conformational changes surrounding residue 386 are due to the differ-

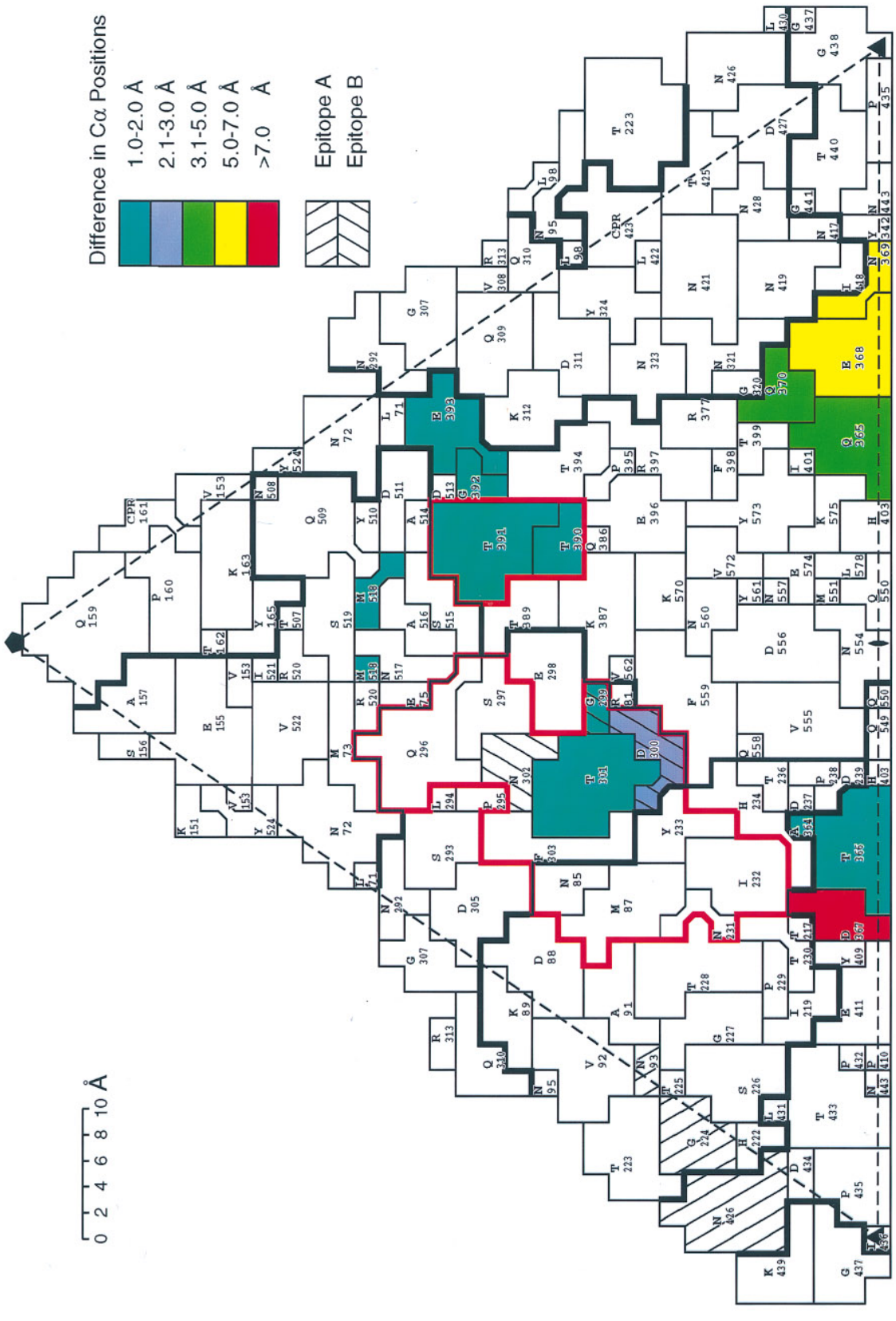

FIG. 4. "Roadmap" of the surface of the CPV-d Ala300 → Asp mutant. Shown is one icosahedral asymmetric unit. The footprint of the Fab fragment of the neutralizing antibody A3B10 is outlined with a heavy red line. Escape mutations for epitopes A and B are shaded. Residues whose C_α positions differ by more than 1.0 Å relative to CPV-Alabama are colored in accordance to the size of the conformational change. Boundaries between different subunits are shown by a heavy black line.

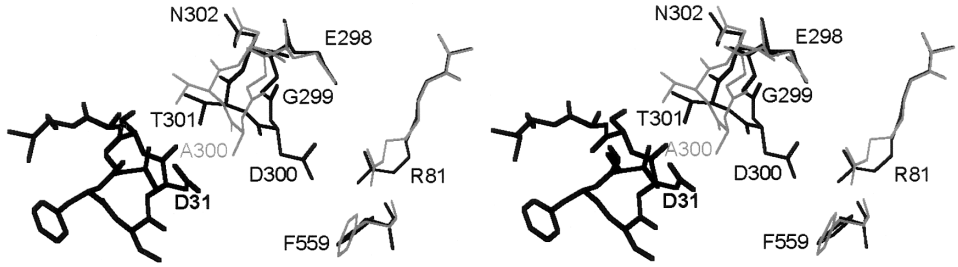

FIG. 3. Stereographic view in which CPV-d structure (thin black) is compared to the CPV-d Ala300 → Asp mutant (gray). Note the shielding of Arg81 by Ala300 in the mutant, which reduces the interaction of MAb (bold black) Asp31 with the CPV residue Arg81.

ence between virus strains and not to the mutation of residue 300 from Ala to Asp.

The change in structure of loop 360 to 373 is puzzling. This surface loop differed in structure between CPV-Alabama (where it was somewhat disordered) and FPV (where it was well ordered). The FPV structure was determined at pH 7.5, where FPV is incapable of hemagglutination, while CPV strains hemagglutinate at all pH's between 6.2 and 7.5. The area covered by the loop is associated with residues that determine the pH dependence of hemagglutination (Chang *et al.,* 1992) and other residues associated with host range in CPV and FPV and tissue tropism in minute virus of mice (Gardiner and Tattersall, 1988; Chang *et al.,* 1992). Thus, it was suggested that this loop is associated with the binding site of viruses to erythrocytes during hemagglutination and has a conformation which is sensitive to pH in FPV. The conditions for hemagglutination by the Ala300 → Asp mutant are similar to those for CPV-Alabama. However, surprisingly, the 359–374 loop displays a conformation similar to FPV (Agbandje *et al.,* 1993). This observation suggests that there is a correlation between residue 386 (Lys in CPV-Alabama and Gln in CPV-d, CPV-d mutant and FPV) and the conformation of this loop. Hence, the correlation between the conformation of the 359–374 loop and hemagglutination has to be reconsidered.

Another region of difference between the mutant and CPV-Alabama is at residue 518, but this is a part of the structure with poor electron density in CPV-Alabama and, thus, may be due to "noise."

The major structural effect of the mutation Ala300 → Asp is the formation of a salt bridge between Asp300 and Arg81 on a threefold-related subunit (Fig. 2). However, docking of HyHel 5, modified by the sequence of the neutralizing MAb A3B10, showed that Asp31 of this antibody might interact with Arg81. Thus, the mutant CPV structure may inhibit this antibody:virus interaction (Fig. 4) by reducing the binding affinity. The escape mutations Gly299 → Glu or Asn302 → Asp (both of which are spatially adjacent to Ala300) would, presumably, form a salt bridge with Arg81 in a manner similar to the Ala300 → Asp mutation, thus blocking the viral interaction with Asp31 of the Fab. The escape mutation Ala300 → Val introduces hydrophobic atoms in between CPV Arg81 and MAb Asp31, which would have an effect much like the Ala300 → Asp mutant structures. In contrast, the mutation Ala300 → Gly does not effect the ability of MAb A3B10 to bind the virus (Strassheim *et al.,* 1994), presumably because neither Ala nor Gly interferes with the charge interaction between virus and antibody. No differences were detectable in host range or antigenicity between CPV-d and CPV-Alabama (C. R. Parrish, unpublished results), indicating that the conformational changes around residue 300 are entirely due to the altered phenotype of the Ala300 → Asp mutant of CPV-d virus.

Mutations that affect host range (Chang *et al.,* 1992; Truyen *et al.,* 1995) have been mostly mapped onto the viral surface (Agbandje *et al.,* 1993; Chapman and Rossmann, 1993). This suggests that host range is determined, in part or completely, by the interaction of the virion with a host factor. Although host range is determined at an early stage after viral attachment, the differentiation appears to occur after cell entry (Horiuchi *et al.,* 1992). The most obvious effect of the Ala300 → Asp mutation is the formation of a salt bridge between three-

TABLE 3

Amino Acid Differences in Selected Parvoviruses

Residue	80	93	103	232	300	323	375	386	484	564	568
CPV-Alabama	R	N	A	I	A	N	N	K	V	S	G
CPV-d								Q			
CPV-d Ala300 → Asp					D			Q			
FPV	K	K	V	V	A	D	D	Q	I	N	A

Note. Blanks indicate residues identical to CPV-Alabama.

fold-related subunits within the capsid, which is likely to increase the viral stability and, therefore, possibly increase the difficulty of uncoating. Preliminary studies (J. S. L. Parker and C. R. Parrish, unpublished results) indicate that the mutation Gly299 → Glu decreases the sensitivity of the virus to urea denaturation. Studies of picornaviruses (Rossmann, 1994) suggest that uncoating can be manipulated by a host "pocket factor," which alters the viral stability. By analogy, similar mechanisms that alter viral stability may occur in parvoviruses and result in differential effects on the ability of the virus to uncoat in various cell types.

ACKNOWLEDGMENTS

We are grateful to our many Purdue colleagues who participated in the data collection trips to CHESS and to the ever helpful CHESS staff. The work was supported by National Institutes of Health grants to C.R.P. and M.G.R. (Grants AI 33468 and AI 11219, respectively), a Spanish Ministry of Education Fellowship to A.L.-S., and a graduate research assistantship from the Cornell University College of Veterinary Medicine to J.S.L.P.

REFERENCES

Agbandje, M., McKenna, R., Rossmann, M. G., Strassheim, M. L., and Parrish, C. R. (1993). Structure determination of feline panleukopenia virus empty particles. *Proteins* 16, 155–171.

Arnold, E., and Rossmann, M. G. (1988). The use of molecular-replacement phases for the refinement of the human rhinovirus 14 structure. *Acta Crystallogr.* A44, 270–282.

Chang, S.-F., Sgro, J.-Y., and Parrish, C. R. (1992). Multiple amino acids in the capsid structure of canine parvovirus coordinately determine the canine host range and specific antigenic and hemagglutination properties. *J. Virol.* 66, 6858–6867.

Chapman, M. S., and Rossmann, M. G. (1993). Structure, sequence and function correlations among parvoviruses. *Virology* 194, 491–508.

Chapman, M. S., and Rossmann, M. G. (1996). Structure refinement of the DNA-containing capsid of canine parvovirus using *RSRef,* a resolution-dependent stereochemically restrained real-space refinement method. *Acta Crystallogr.* D52, 129–140.

Cotmore, S. F., and Tattersall, P. (1987). The autonomously replicating parvoviruses of vertebrates. *Adv. Virus Res.* 33, 91–174.

Gardiner, E. M., and Tattersall, P. (1988). Mapping the fibrotropic and lymphotropic host range determinants of the parvovirus minute virus of mice. *J. Virol.* 62, 2605–2613.

Horiuchi, M., Ishiguro, N., Goto, H., and Shinagawa, M. (1992). Characterization of the stage(s) in the virus replication cycle at which the host-cell specificity of the feline parvovirus sub-group is regulated in canine cells. *Virology* 189, 600–608.

Jongeneel, C. V., Sahli, R., McMaster, G. K., and Hirt, B. (1986). A precise map of splice junctions in the mRNA's of minute virus of mice, an autonomous parvovirus. *J. Virol.* 59, 564–573.

Kunkel, T. A. (1985). Rapid and efficient site-specific mutagenesis without phenotypic selection. *Proc. Natl. Acad. Sci. USA* 82, 488–492.

Langeveld, J. P. M., Casal, J. I., Vela, C., Dalsgaard, K., Smale, S. H., Puijk, W. C., and Meloen, R. H. (1993). B-cell epitopes of canine parvovirus: distribution of the primary structure and exposure on the viral surface. *J. Virol.* 67, 765–772.

López de Turiso, J. A., Cortés, E., Ranz, A., Garcia, J., Sanz, A., Vela, C., and Casal, J. I. (1991). Fine mapping of canine parvovirus B cell epitopes. *J. Gen. Virol.* 72, 2445–2456.

Matthews, B. W. (1968). Solvent content of protein crystals. *J. Mol. Biol.* 33, 491–497.

McPherson, A. (1982). "Preparation and Analysis of Protein Crystals." Wiley, New York.

Nichols, G. E., Shiraishi, T., and Young Jr., W. W. (1988). Polarity of neutral glycolipids, gangliosides, and sulfated lipids in MDCK epithelial cells. *J. Lipid Res.* 29, 1205–1213.

Otwinowski, Z. (1993). DENZO. *In* "Data Collection and Processing" (L. Sawyer, N. Isaacs, and S. Bailey, Ed.), pp. 56–62. SERC Daresbury Laboratory, Warrington, UK.

Parrish, C. R. (1990). Emergence, natural history, and variation of canine, mink and feline parvoviruses. *Adv. Virus Res.* 38, 403–450.

Parrish, C. R. (1991). Mapping specific functions in the capsid structure of canine parvovirus and feline panleukopenia virus using infectious plasmid clones. *Virology* 183, 195–205.

Parrish, C. R., and Carmichael, L. E. (1986). Characterization and recombination mapping of an antigenic and host range mutation of canine parvovirus. *Virology* 148, 121–132.

Parrish, C. R., Aquadro, C., Strassheim, M. L., Evermann, J. F., Sgro, J.-Y., and Mohammed, H. O. (1991). Rapid antigenic-type replacement and DNA sequence evolution of canine parvovirus. *J. Virol.* 65, 6544–6552.

Rimmelzwaan, G., Carlson, J., UytdeHaag, F. G., and Osterhaus, A. D. (1990). A synthetic peptide derived from the amino acid sequence of canine parvovirus structural proteins which defines a B cell epitope and elicits antiviral antibody in BALB c mice. *J. Gen. Virol.* 71, 2741–2745.

Rossmann, M. G. (1979). Processing oscillation diffraction data for very large unit cells with an automatic convolution technique and profile fitting. *J. Appl. Crystallogr.* 12, 225–238.

Rossmann, M. G. (1994). Viral cell recognition and entry. *Protein Sci.* 3, 1712–1725.

Rossmann, M. G., and Blow, D. M. (1962). The detection of sub-units within the crystallographic asymmetric unit. *Acta Crystallogr.* 15, 24–31.

Rossmann, M. G., and Johnson, J. E. (1989). Icosahedral RNA virus structure. *Annu. Rev. Biochem.* 58, 533–573.

Rossmann, M. G., Leslie, A. G. W., Abdel-Meguid, S. S., and Tsukihara, T. (1979). Processing and post-refinement of oscillation camera data. *J. Appl. Crystallogr.* 12, 570–581.

Rossmann, M. G., McKenna, R., Tong, L., Xia, D., Dai, J., Wu, H., Choi, H. K., and Lynch, R. E. (1992). Molecular replacement real-space averaging. *J. Appl. Crystallogr.* 25, 166–180.

Siegl, G. (1984). Biology and pathogenicity of autonomous parvoviruses. *In* "The Parvoviruses" (K. I. Berns, Ed.), pp. 297–362. Plenum Press, New York/London.

Strassheim, M. L., Gruenberg, A., Veijalainen, P., Sgro, J.-Y., and Parrish, C. R. (1994). Two dominant neutralizing antigen determinants of canine parvovirus are found on the threefold spike of the virus capsid. *Virology* 198, 175–184.

Truyen, U., Gruenberg, A., Chang, S.-F., Obermaier, B., Veijalainen, P., and Parrish, C. R. (1995). Evolution of the feline-subgroup parvoviruses and the control of canine host range *in vivo.* *J. Virol.* 69, 4702–4710.

Truyen, U., Evermann, J. F., Vieler, E., and Parrish, C. R. (1996). Evolution of canine parvovirus involved in loss and gain of feline host range. *Virology* 215, 186–189.

Tsao, J., Chapman, M. S., Agbandje, M., Keller, W., Smith, K., Wu, H., Luo, M., Smith, T. J., Rossmann, M. G., Compans, R. W., and Parrish, C. R. (1991). The three-dimensional structure of canine parvovirus and its functional implications. *Science* 251, 1456–1464.

Tsao, J., Chapman, M. S., Wu, H., Agbandje, M., Keller, W., and Rossmann, M. G. (1992). Structure determination of monoclinic canine parvovirus. *Acta Crystallogr.* B48, 75–88.

Wikoff, W. R., Wang, G., Parrish, C. R., Cheng, R. H., Strassheim, M. L., Baker, T. S., and Rossmann, M. G. (1994). The structure of a neutralized virus: canine parvovirus complexed with neutralizing antibody fragment. *Structure* 2, 595–607.